Extended Data Figures and Supplementary Movies

Geometry-driven migration efficiency of minimal cell clusters

Eléonore Vercurysse[#1], David B. Brückner[#2], Manuel Gómez-González[3], Marine Luciano[1], Yohalie Kalukula[1], Leone Rossetti[3], Xavier Trepat[3,4,5,6], Edouard Hannezo[2*] and Sylvain Gabriele[1*]

[1] Mechanobiology & Biomaterials group, Interfaces and Complex Fluids Laboratory, Research Institute for Biosciences, CIRMAP, University of Mons, Place du Parc, 20 B-7000 Mons, Belgium

[2] Institute for Science and Technology Austria. Am Campus 1, A-3400 Klosterneuburg, Austria

[3] Institute for Bioengineering of Catalonia (IBEC), The Barcelona Institute for Science and Technology (BIST), 08028 Barcelona, Spain.

[4] Centro de Investigación Biomédica en Red en Bioingeniería, Biomateriales y Nanomedicina (CIBER-BBN), 08028 Barcelona, Spain.

[5] Facultat de Medicina, Universitat de Barcelona, 08036 Barcelona, Spain.

[6] Institució Catalana de Recerca i Estudis Avançats (ICREA), Barcelona, Spain.

[#]Contributed equally to this work

*To whom correspondence should be addressed: edouard.hannezo@ist.ac.at and sylvain.gabriele@umons.ac.be

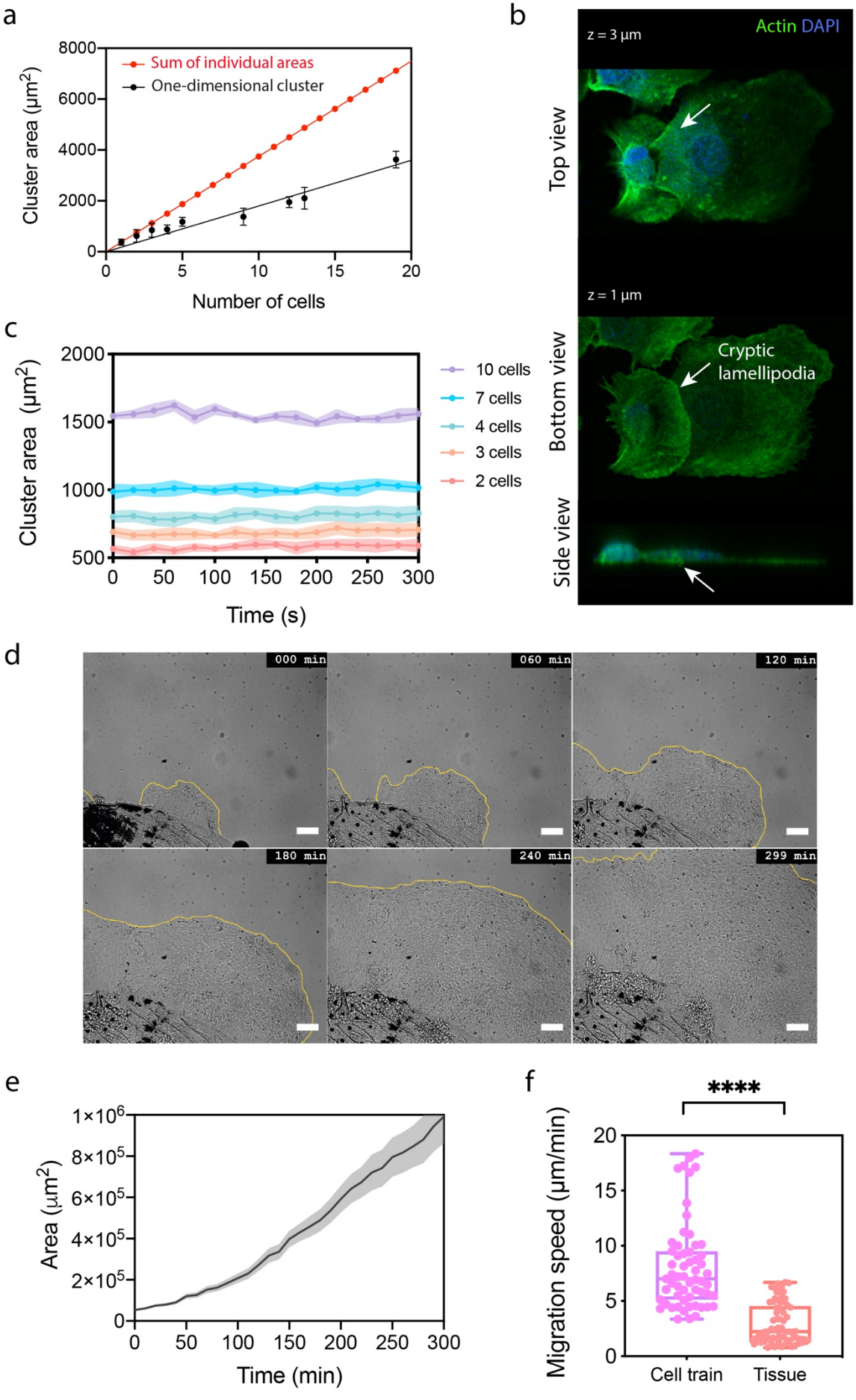
a
Cluster area (μm²)
8000
6000
4000
2000
0
Sum of individual areas
One-dimensional cluster
0
5
10
15
20
Number of cells
b
z = 3 μm
Actin DAPI
Top view
z = 1 μm
Bottom view
Cryptic lamellipodia
Side view
c
Cluster area (μm²)
2000
1500
1000
500
10 cells
7 cells
4 cells
3 cells
2 cells
0
50
100
150
200
250
300
Time (s)
d
000 min
060 min
120 min
180 min
240 min
299 min
e
Area (μm²)
1×10⁶
8×10⁵
6×10⁵
4×10⁵
2×10⁵
0
0
50
100
150
200
250
300
Time (min)
f
****
Migration speed (μm/min)
20
15
10
5
0
Cell train
Tissue

Extended Data Figure 1 – One-dimensional epithelial clusters are compacted and faster than tissues. (a) The cluster area is linearly correlated with the number of cells (black points) and smaller than the sum of individual cell areas (red points), suggesting that cells in one-dimensional epithelial clusters are significantly compacted. **(b)** Confocal images (top, bottom, and side views) of a cryptic lamellipodia in a cell doublet. **(c)** The cluster area is constant over time, regardless the number of cells, demonstrating that one-dimensional epithelial clusters move as a single unit. **(d)** Typical time-lapse sequence in DIC mode of a bidimensional epithelial tissue growing out of a scale during 299 min. The growing front is depicted with a yellow line. The scale bar is 100 µm. **(e)** Evolution of the tissue area over time (n=3, mean ± S.D.). **(f)** Migration speed for one-dimensional epithelial clusters ("cell train" in pink, n=62) and epithelial tissues ("tissue" in red, n=74) with ****$p < 0.0001$.

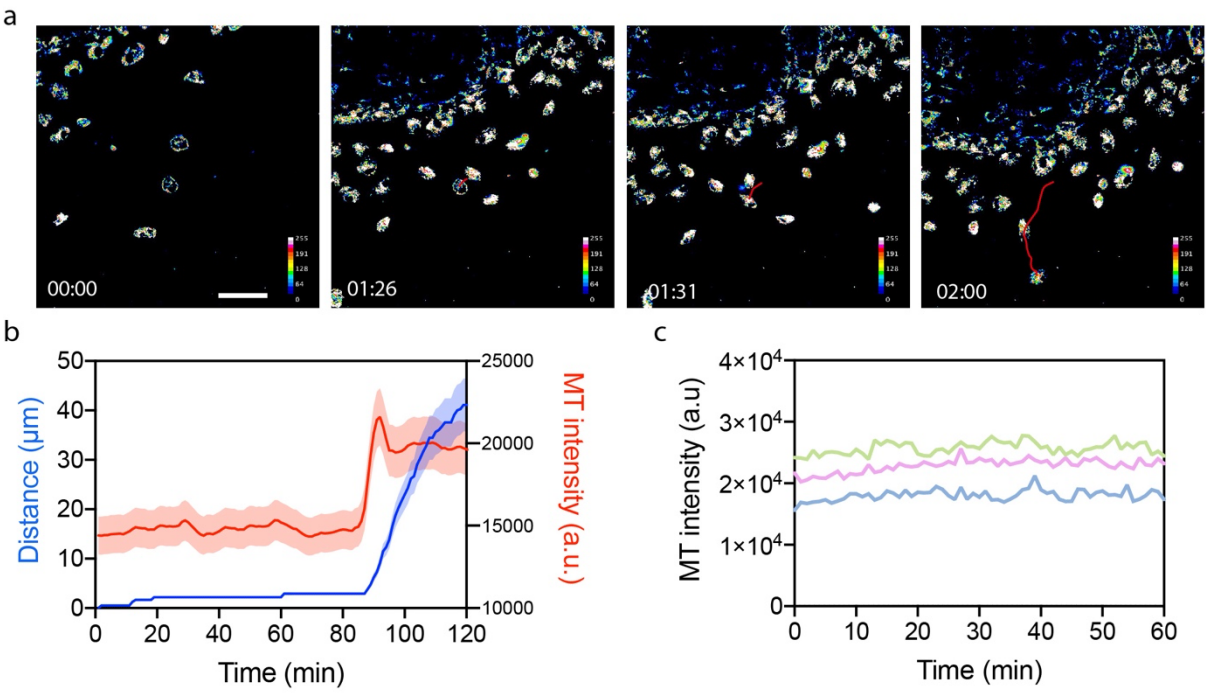

Extended Data Figure 2 – The mitochondrial membrane potential increases as the cell polarizes and remains constant during migration. (a) Typical time-lapse sequence in epifluorescence mode of single epithelial cells stained with red MitoTracker (MT). Cells were digitized in 256 bits and the MitoTracker intensity was color-coded (from high to low: white, purple, red, orange, yellow, green, light blue and dark blue). The redline shows the displacement of a cell that started to polarize and migrate at 86 min. The scale bar is 30 µm. **(b)** Evolution of the distance (in blue) and the MT intensity (in red) over time (n=3, mean ± S.D.) **(c)** Evolution of the MT intensity of three individual polarized cells that migrate during 60 min.

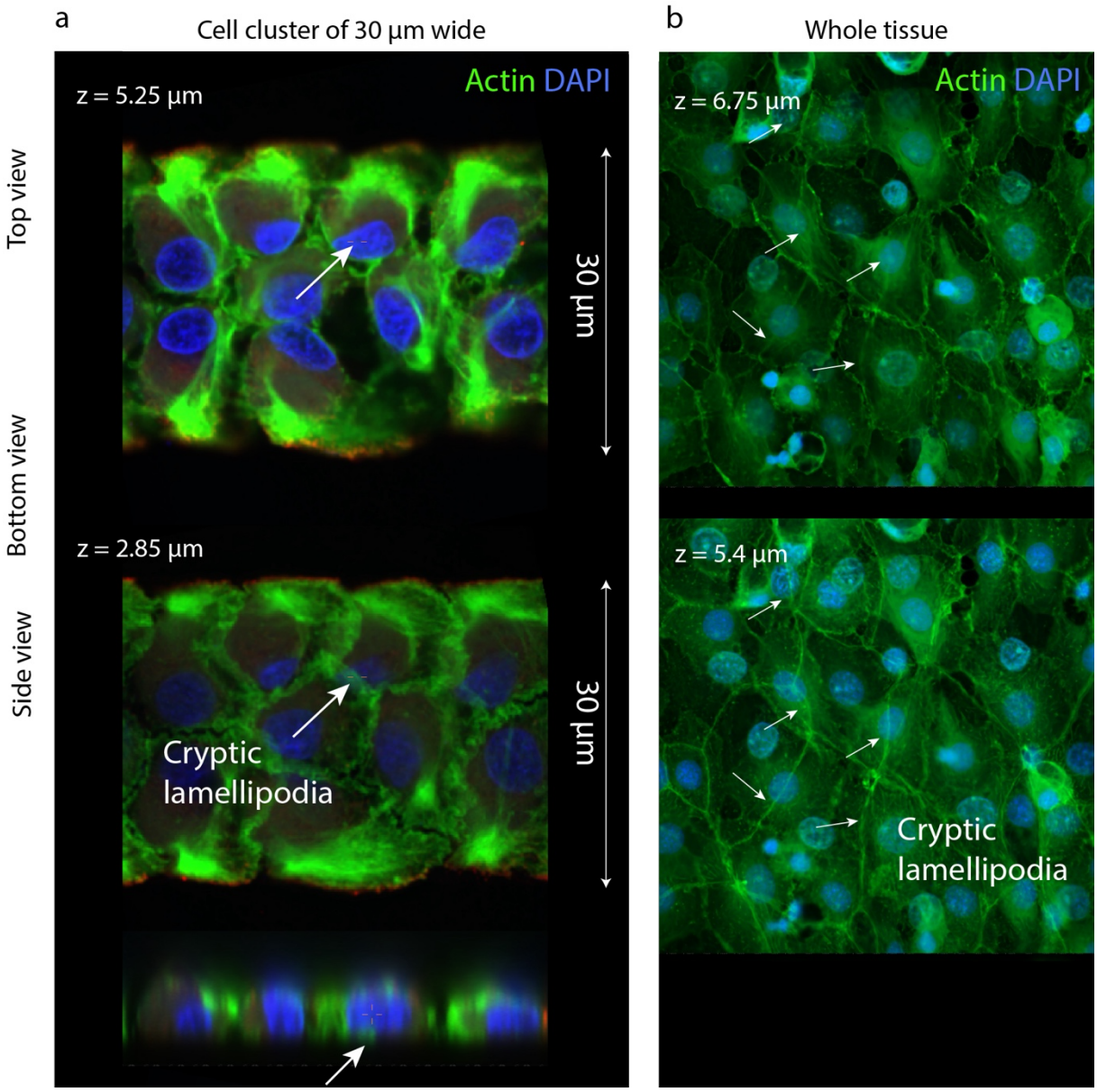

Extended Data Figure 3 – Cell clusters and epithelial tissues are composed of cryptic lamellipodia that invade underneath the adjoining cell. Confocal images (top, bottom, and side views) of cryptic lamellipodia in **(a)** an epithelial cluster of 30 µm wide and **(b)** a bidimensional epithelial tissue. Actin is labeled in green with Phalloidin and DNA in blue with DAPI. The white arrows show the position of typical cryptical lamellipodia.

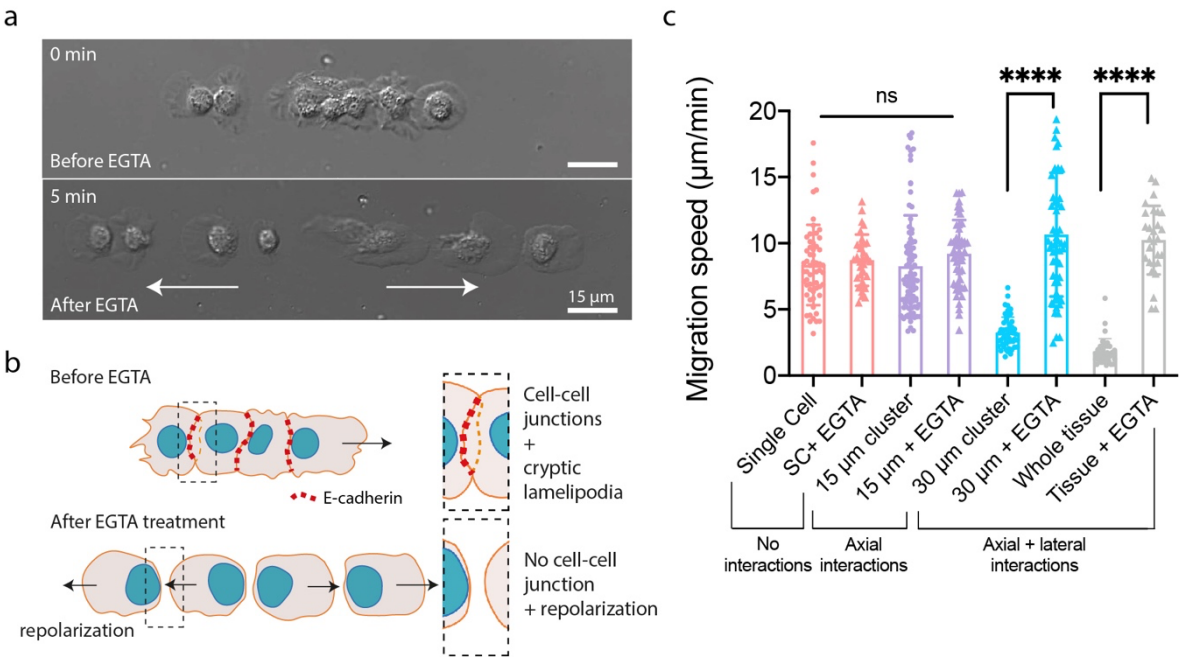

Extended Data Figure 4 – Disruption of cell-cell adhesions with EGTA treatments leads to the increase of the migration speed and repolarization events. (a) Typical microscopy images in DIC mode of a one-dimensional epithelial cluster migrating on a 15 µm wide micropatterns before (t=0 min) and after (t=5 min) EGTA treatments. White arrows show the cell repolarization. Scale bars are 15 µm. **(b)** Schematic representation of the EGTA effect that disrupts adherens cell-cell adhesions due to a weakening of the rigid extracellular domain of E-cadherin and leads to repolarization events. **(c)** Migration speed of single cells on 15 µm wide microstripes (control: n=57, EGTA: n=32, in red), cell trains on 15 µm wide microstripes (control: n=88, EGTA: n= 49, in purple), epithelial clusters on 30 µm wide microstripes (control: n=51, EGTA: n=57, in blue) and whole epithelial tissues (control: n=37, EGTA: n=28, in grey). Control data are circles and EGTA-treated data are lozenges, ns is non-significant and ****$p < 0.0001$.

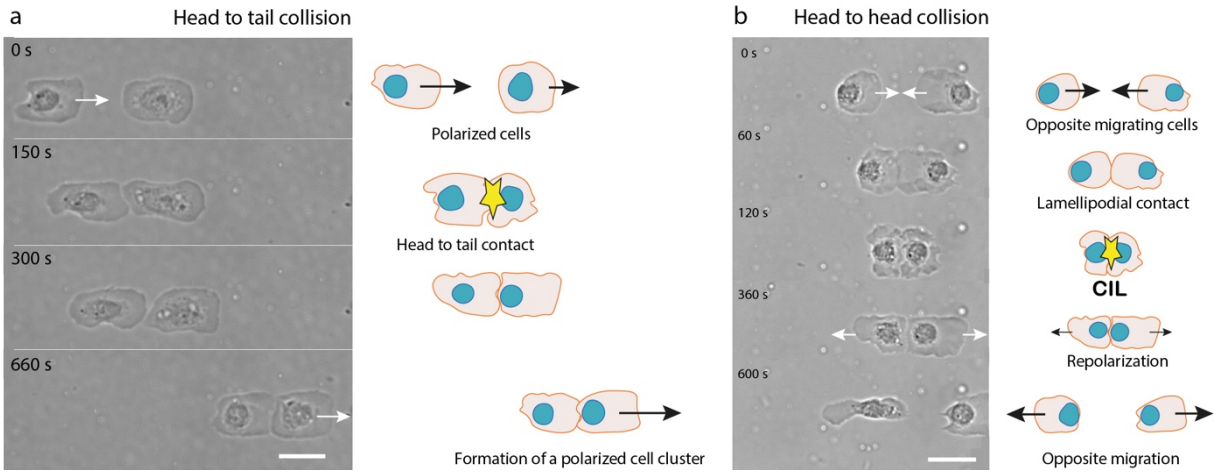

Extended Data Figure 5 – The collision configuration between two epithelial cells induced an attractive or repulsive response. (a) Head-to-tail collisions promoted to the formation of a contact between a cell lamellipodia and the tail of a neighboring cell, leading to the formation of a polarized cell doublet, suggesting that head-to-tail collisions can promote the formation of larger cell clusters. **(b)** The contact inhibition of locomotion (CIL) was observed during head-to-head collisions between individual epithelial cells moving on 15 µm wide, showing a repulsive response of both cells that repolarized rapidly in opposite directions.

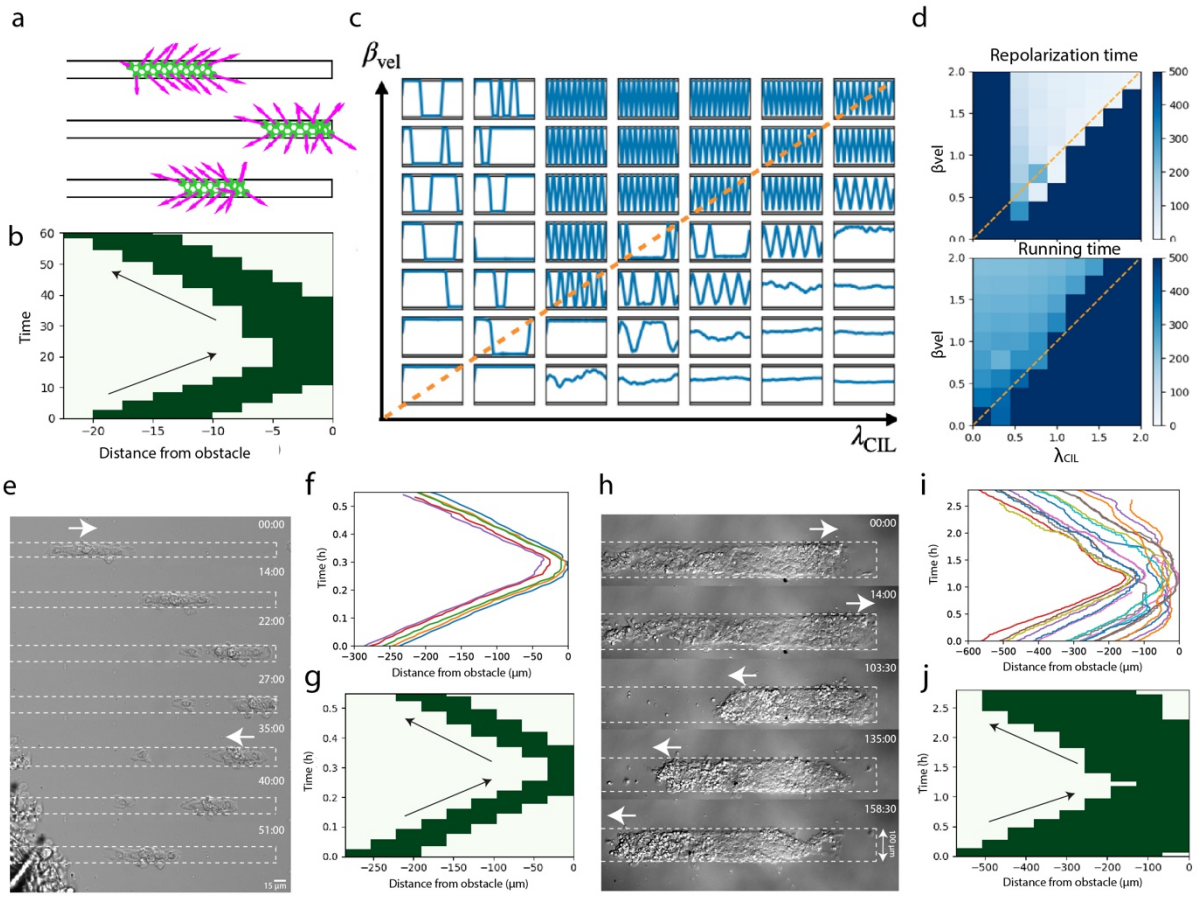

Extended Data Figure 6 – Perturbation of the polarization of epithelial cell clusters by migrating against an obstacle. (a) Theoretical simulation of the migration of a one-dimensional epithelial cluster migrating from the left to the right towards an obstacle. By using the combination of VA+PA+CIL we can observe that the cell train repolarizes towards the opposite direction after the collision. **(b)** Kymograph of the spatial position over time of the simulated cell train in (a), showing its repolarization after the collision. The slopes before and after the collision indicated similar migrating velocities. **(c)** Phase diagram showing trajectories of cell cluster center of mass in obstacles at both ends of the microstrip, as a function of the interaction parameters β_{vel} and λ_{CIL}. **(d)** Phase diagrams of repolarization and running times as a function of β_{vel} and λ_{CIL}, quantifying the repolarization and running phases in panel c. **(e)** Time-lapse sequence of the migration of a one-dimensional cluster moving towards the border of a 15 µm-wide fibronectin microstripe (from left to right) during 51 min. After reaching the micropattern extremity on the left part, the cell train compacted against the border, then

epithelial cells repolarized and the cluster migrated in the opposite direction (from right to left). **(f)** Distance travelled over time by individual cells within the cell train presented in (e). Each color-coded line corresponds to the one cell. **(g)** Kymograph of the spatial position over time of the cell train presented in (e), showing its repolarization after the collision. The slopes before and after the collision indicated similar migrating velocities. **(h)** Time-lapse sequence of the migration of a 100 µm wide epithelial cluster moving towards the border of a fibronectin microstripe (left to the right) during 158 min. After reaching the micropattern extremity on the left part, the wide cluster compacted against the border, then epithelial cells repolarized and the whole cluster migrated in the opposite direction (right to left). **(i)** Distance travelled over time by individual cells within the 100 µm wide cluster presented in (h). Each color-coded line corresponds to the one cell. **(j)** Kymograph of the spatial position over time of the 100 µm wide cluster presented in (h), showing its repolarization after the collision. The slopes before and after the collision indicated similar migrating velocities.

Supplementary Movie S1. Time-lapse sequence in DIC mode of a polarized one-dimensional cluster (7 polarized cells) that migrated on a 15 μm wide fibronectin micropattern. The scale bar is 10 μm.

Supplementary Movie S2. Time-lapse sequence in DIC mode of a polarized one-dimensional cluster (10 polarized cells) that migrated on a 15 μm wide fibronectin micropattern. The scale bar is 10 μm.

Supplementary Movie S3. Time-lapse sequence in epifluorescence mode of epithelial keratocytes labelled with the MitoTracker (MT) Red dye. Cells were detached from the front edge of primary tissue growing from the fish scale. The fluorescence intensity of the dye was proportional to the mitochondrial membrane potential. Unpolarized and stationary cells showed a low MT fluorescence intensity, which increased immediately with their polarization and migratory state. Cells were digitized in 256 bits and the MT intensity was color-coded (from high to low: white, purple, red, orange, yellow, green, light blue and dark blue). The total duration time is 1 hour and 59 minutes.

Supplementary Movie S4. Time-lapse sequence in DIC mode of a polarized epithelial cluster that migrates on a 35 μm wide fibronectin micropattern. The scale bar is 25 μm.

Supplementary Movie S5. Time-lapse sequence in DIC mode of polarized epithelial cluster that migrates on a 50 μm wide fibronectin micropattern. The scale bar is 25 μm.

Supplementary Movie S6. Animated simulations of the model with single interaction types; from top to bottom: polarity alignment (PA), velocity alignment (VA), stress-polarity coupling

(SPC), contact inhibition of locomotion (CIL). Green dots: cell positions, green lines: elastic links between cells, magenta arrows: polarities. Cells were initialized with random polarities.

Supplementary Movie S7. Animated simulations of the model with pair-wise combinations of interactions; from top to bottom: VA+SPC, PA+SPC, VA+CIL, PA+CIL. Green dots: cell positions, green lines: elastic links between cells, magenta arrows: polarities. Cells were initialized with random polarities.

Supplementary Movie S8. Animated simulations of the model combining velocity alignment, polarity alignment, and contact inhibition of locomotion (VA+PA+CIL). Green dots: cell positions, green lines: elastic links between cells, magenta arrows: polarities. Cells were initialized with random polarities. From top to bottom, systems with increasing width are shown, corresponding to n = 1,2,3,4 cells.

Supplementary Movie S9. Animated simulations of the repolarization behavior of model in a confined system with various interaction mechanisms. From top to bottom, the interaction mechanisms PA, VA, VA+CIL, VA+PA+CIL are shown. Green dots: cell positions, green lines: elastic links between cells, magenta arrows: polarities. Cells were initialized with random polarities.

Supplementary Movie S11. Animated simulations of the model combining velocity alignment, polarity alignment, and contact inhibition of locomotion (VA+PA+CIL), with parameters that capture the qualitative behavior of MDCK cell clusters. Top: microstripe (open boundary conditions). Bottom: microring (periodic boundary conditions). Green dots: cell positions,

green lines: elastic links between cells, magenta arrows: polarities. Cells were initialized with random polarities.